



Coupling of double grains enforces the grinding process in vibration-assisted scratch: Insights from molecular dynamics

Zhongwei Hu^{a,b}, Yue Chen^{a,b}, Zhiyuan Lai^{a,b}, Yiqing Yu^{b,*}, Xipeng Xu^{a,b}, Qing Peng^d, Long Zhang^c

^a Institute of Manufacturing Engineering, Huaqiao University, Xiamen 361021, China

^b Institute of Mechanical Engineering and Automation, Huaqiao University, Xiamen 361021, China

^c State Key Laboratory of Mechanical System and Vibration, Shanghai Jiao Tong University, Shanghai 200240, China

^d State Key Laboratory of Nonlinear Mechanics, Institute of Mechanics, Chinese Academy of Sciences, Beijing 100190, China

ARTICLE INFO

Associate Editor: Erhan Budak

Keywords:

Single-crystal silicon carbide
Vibration-assisted scratch
Double abrasive grains
Molecular dynamics

ABSTRACT

Coupling of multiple abrasive grains is crucial for the efficiency in the grinding process and grinder design. Here the coupling effect in a double-grain model in vibration-assisted scratch of single-crystal silicon carbide (SiC) have been investigated using the molecular dynamics simulations for both simultaneous and sequential scratch processes. The coupling between the double abrasive grains affect the scratch force, stress, amorphous layer and surface morphology. The reduction ratios of tangential and normal force and the influenced material volume show that the critical distance for the inhibition of the coupling of vibration-assisted scratch is significantly greater than that in conventional scratch. The change of overlap ratio can reflect the change trend of the scratch force reduction ratio. In the vibration-assisted grinding, the increase of overlap ratio also intensifies the coupling of the abrasive grains, resulting in faster material removal, smaller scratch force and better surface finish. Insights obtained through the molecular dynamics analysis in this work into the coupling effects of abrasive grains in the vibration-assisted grinding process is believed to be beneficial in the development of grinding wheels and the optimization of machining processes.

1. Introduction

Semiconductor materials are usually hard and brittle materials, which make machining difficult (Wu et al., 2020). At present, grinding is the most economic and widely used method for processing hard and brittle materials (Huang et al., 2021). However, it is still challenging to obtain high-efficiency and high-quality machining outputs (Sharma et al., 2021). Vibration-assisted grinding is an effective method for precision machining of hard and brittle materials realized via the application of a certain frequency and amplitude to the workpiece or grinding wheel on the basis of conventional grinding (Kumar, 2013). Compared with conventional grinding, Wen et al. (2019) found that the surface contact stiffness of the vibration-assisted grinding surface was significantly improved. And Cao et al. (2014) found that the maximum local contact pressure reduced and the stiffness of the experimental device was improved. Moreover, vibration-assisted grinding can reduce the grinding force (Yang et al., 2019b), surface roughness (Zhou et al., 2019b), and subsurface damage (Baraheni and Amini, 2019), as well as

improve the material removal rate (Qu et al., 2000). It results from the comprehensive action of a multitude of discrete abrasive grains on the surface of a workpiece. As multiple abrasive grains simultaneously interact with the workpiece surface, grinding is a complex process. To study the grinding mechanisms, it is common to start with a single abrasive grain scratch, integrate the scratch results of a single abrasive in the grinding influence area effectively, and subsequently analyze various physical phenomena in the grinding process (Zheng et al., 2018). However, in the grinding process, both direct coupling between the abrasive grains and the workpiece and indirect coupling between the adjacent abrasive grains on the workpiece exist. Therefore, to study the grinding mechanism, the coupling between the abrasive grains must be studied.

To study the indirect coupling between the abrasive grains, multi-scratch experiments were conducted (Yang and Gao, 2022). In the process, owing to the different positional relationship of the abrasive grain arrangement, when passing through the workpiece, two abrasive grains were arranged to simultaneously (Feng et al., 2020). or

* Corresponding author.

E-mail address: yyqing@hqu.edu.cn (Y. Yu).

<https://doi.org/10.1016/j.jmatprotec.2022.117551>

Received 30 January 2022; Received in revised form 22 February 2022; Accepted 6 March 2022

Available online 10 March 2022

0924-0136/© 2022 Elsevier B.V. All rights reserved.

sequentially scratch (Duan et al., 2017) the workpiece. Different scratch characteristics can be obtained by simultaneous scratch compared to sequential scratch. During the actual experiments, Feng et al. (2020) have performed simultaneous scratch with double tips fabricated using a focus ion beam, while Dai et al. (2019) was used a rotating clamping double abrasive device to adjust the axial distance of the abrasive grains for the sequential scratch. The spacing of the abrasive grains (Gu et al., 2011), tool apex angle (Feng et al., 2019) and the scratch depth (Qiu et al., 2016) influence the effect of the coupling between the two scratches on the scratch force, maximum principal stress, and material removal rate. Cai et al. (2019) found the lateral crack coupling between the double scratches resulted in the overall removal of the workpiece material and the slip of the second scratch. And with the increase spacing of the scratches, Wang et al. (2019) found the radial crack was easier to propagate. In the sequential scratch, Yang et al. (2019a) found the maximum principal stress promoted the serious crack propagation in the workpiece. Further, Geng et al. (2014) have studied the relationship between the normal load and groove depth. However, owing to the limitations of the existing technology and experiment equipment, conducting a comprehensive and systematic vibration-assisted multiple abrasive grains scratch experiment is challenging, which has hindered the research on the mechanism of vibration-assisted grinding.

Molecular dynamics (MD) simulation is an effective method for studying the ultrahigh-precision grinding mechanism (Chen et al., 2021) and the change of the material microstructure (Peng et al., 2018). Recently, Chavoshi and Luo (2016a) has been employed to simulate single abrasive grain using MD simulations and Meng et al. (2019) have conducted multiple abrasive grains grinding processes to reveal the mechanism of grinding. In the scratch of single abrasive grain, the focus of research was primarily on the interaction relationship between the abrasive grain and the workpiece. Li et al. (2015) have studied the effect of grinding speed on subsurface damage and grinding surface integrity. And Chavoshi and Xu (2019) have studied the mechanical response of crystalline and amorphous materials subjected to nano-indentation/scratch. Further, in the scratch of multiple abrasive grains, the MD model of two abrasive grains scratched sequentially (Meng et al., 2019) and simultaneously (Zhang et al., 2013) were established. At present, research is focused on the analysis of the surface morphology and damage distribution after double-abrasive scratches. Meng et al. (2019) found that the distance between the abrasive grains and the depth of cut directly affected the characteristics of the machined surface and Zhou et al. (2019a) found that the distance and depth also affected the number of phase-change atoms. Karkalos et al. (2017) found that the wear was primarily conducted by the first abrasive grain, whereas the second abrasive grain removed a small amount of material left owing to the coupling between the first abrasive grain and the surface of the workpiece. Based on previous research, the extent of mutual influence between two abrasive grains in the simultaneous scratch process was evaluated, and in the sequential scratch, the effects of scratch force, stress, and amorphous region morphology of the second abrasive grains were studied and analyzed in detail.

Further, in vibration-assisted scratch (VS), the coupling of adjacent abrasive grains on the workpiece has not been systematically studied. Thus, in this study, the MD method was employed to simulate the VS of SiC with two abrasive grains. Moreover, by analyzing the differences in the scratch force, stress, surface morphology and volume of the influenced material with and without vibration, the extent of coupling between the two abrasive grains during conventional scratch (CS) and VS were evaluated. In addition, the effects of different scratch modes of simultaneous and sequential scratches with different abrasive grain spacings on the scratch process was also studied. The simulation results are significant for the design of the abrasive grain arrangement of the grinding wheel.

2. Molecular dynamic simulations

2.1. Scratch modes setup

To analyze the coupling between abrasive grains in VS and to determine the mechanism of vibration-assisted grinding, the different scratch modes are need to be designed, which should include as much as possible the situations that may occur in the actual processing. In the simulation process, the setting of scratch modes needs to consider the distribution of abrasive grains on the grinding wheel in the actual grinding process. There are four main grinding types: single-sided, self-rotating, double-sided and end-face grinding, as shown in Fig. 1(a). No matter what type of grinding, it is essentially the joint action of a large number of abrasive grains on the workpiece. Considering the nano scale, the abrasive grains can be regarded as spherical. And the positional relationship of the abrasive grains was simplified according to the actual arrangement of the abrasive grains, as shown in Fig. 1(b). The scratch modes were classified corresponding to the position relationship of the abrasive grains: (1) simultaneous scratch: when two abrasive grains are placed side-by-side on the grinding wheel, that is, the distance s in the X direction is 0; at this time the two abrasive grains pass through the workpiece simultaneous, as shown in Fig. 1(c). (2) sequential scratch: when two abrasive grains are arranged sequentially on the grinding wheel, that is, the distance s in the X direction was not 0, and the two abrasive grains passed through the workpiece in a sequential manner, and the workpiece was processed in sequence, as shown in Fig. 1(d). When the distance d between the two abrasive grains in the Y direction was different, the trajectories of the two abrasive grains on the workpiece overlapped completely ($d=0$), partially overlapped ($0 < d < r$) or did not overlap at all ($d > r$).

The essential difference between simultaneous scratch and sequential scratch is whether the two abrasive grains process the workpiece at the same time. Therefore, in the process of simultaneous scratch, the scratch process of the two abrasive grains is affected at the same time. While in the process of sequential scratch, only the scratch process of the second abrasive grain is changed, just the scratch process of the second abrasive grain needs to be analyzed.

In the process of VS, the motion equation of the abrasive grain in the X-direction was: $D_x = v_x t$, and that in the Y-direction was: $D_y = A \sin(2\pi f t)$. For $s = 0$ (i.e., simultaneous scratch), the two abrasive grains moved simultaneously, and the vibration trajectory direction must be consistent. When $s \neq 0$ (i.e., sequential scratch), there may be a phase difference of trajectories, when the abrasive grains across the workpiece. Therefore, two special conditions were considered for the simulation: (1) in-phase scratch: when the s is an integral multiple of the length of a vibration cycle, that is, the distance $s = n/2 * L$, (n is an even number). The trajectory directions of the two abrasive grains on the workpiece are the same; (2) reversed scratch: when s is more than half a cycle of the length of a vibration cycle, that is, $s = n/2 * L$, (n is an odd number). Here, the trajectory directions of the two abrasive grains on the workpiece were opposite, as shown in Fig. 1(d). These two positions are two extreme conditions, and the results of other phase differences are between the two, so these two special positions are selected for research. Based on the possible position relationship between the abrasive grains on the grinding wheel, the simulations are summarized in Table 1.

2.2. MD model setup

In this paper, SiC, as the third-generation semiconductor material, was selected as the workpiece material. Molecular dynamics (MD) method was employed to simulate the VS process of SiC to study the mechanism. First, the scratch model of two abrasive grains was set up, as presented in Fig. 2(a) and (b) showed the simulation models of simultaneous scratch and sequential scratch, respectively. The workpiece was single crystal SiC with a length of 20 nm, width of 38 nm, and height of

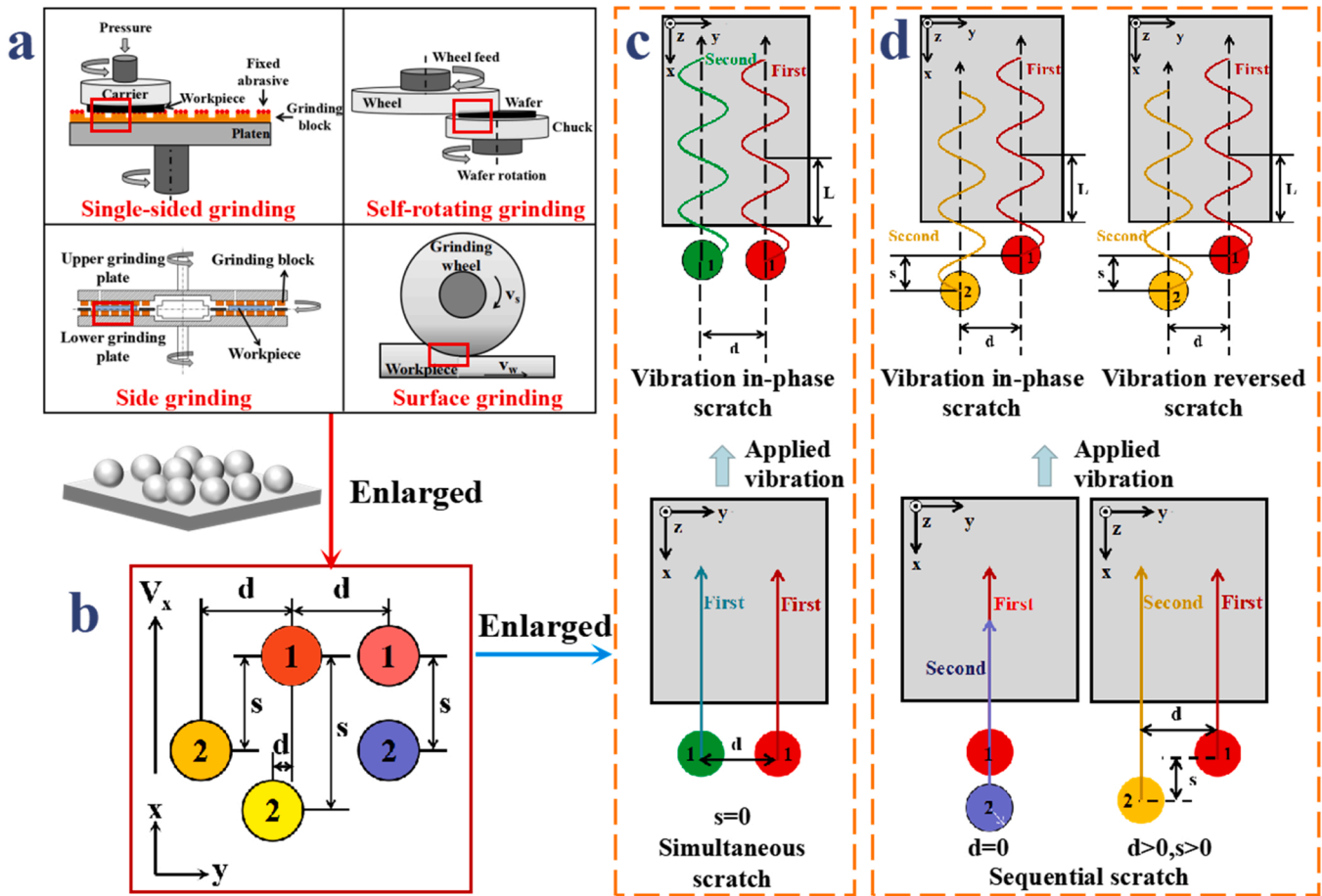


Fig. 1. Schematic diagram of scratch design. (a) Common grinding method, (b) arrangement of abrasive grains after partial (the part of the red box in (a)) magnification, (c) the movement of abrasive grains in the process of simultaneous scratch, (d) the movement of abrasive grains in the process of sequential scratch and (e) in the process of sequential scratch, after applying vibration, the vibration direction may be the same or opposite at the workpiece.

Table 1
Summary of scratch conditions.

Scratch modes		Abrasive grains spacing d in Y direction (nm)
Simultaneous scratch	Conventional scratch	4, 6, 8, 10, 12, 14
	Vibration in-phase scratch $s = n/2 * L$ ($n = \text{even number}$)	4, 6, 8, 10, 12, 14
Sequential scratch	Conventional scratch	0, 2, 4, 6, 8, 10, 12, 14
	Vibration in-phase scratch $s = n/2 * L$ ($n = \text{even number}$)	0, 2, 4, 6, 8, 10, 12, 14
	Vibration reversed scratch $s = n/2 * L$ ($n = \text{odd number}$)	0, 2, 4, 6, 8, 10, 12, 14

7.8 nm. The workpiece model consisted of three layers: a boundary layer, thermostat layer, and a Newtonian layer. Further, the abrasive grain material was diamond with a perfect lattice, considering that it is in nano scale, the shape of abrasive grains was simplified to the combination of a hemisphere (radius was 2 nm) and a cylinder (height was 2.2 nm), which was regarded as a rigid body, and its wear was not considered. The entire simulation model included 597074 atoms (including 588059 atoms of the workpiece). All the MD simulations were performed using a large-scale atom molecule parallel simulator (LAMMPS) (Plimpton, 1995), and visualization and snapshot generation of MD simulation data were using by OVITO (Stukowski, 2010). Because the selection of the potential function is crucial for ensuring accurate simulation results, the Tersoff potential function—which can accurately describe the coupling between atoms of covalent systems such as C and Si (Tersoff, J., 1989)—of multi-atom system was used to simulate single crystal Si, diamond C-C, and Si-C. In this model, the influence of size

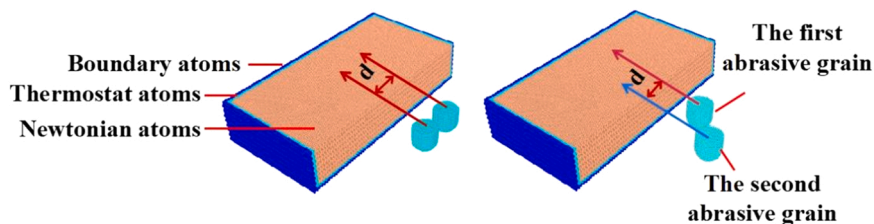


Fig. 2. A schematic of the MD simulation model and model display of some scratch modes models: (a) simultaneous scratch and (b) sequential scratch at abrasive lateral spacing is six.

effect was ignored (Dulak et al., 2011).

In the scratch process, NVT and NVE ensemble were applied to thermostat atoms layer and Newtonian atoms layer, respectively. And the abrasive grains are on the (0001) surface of SiC along the [1–210] direction. Owing to the consideration of technical resources and calculation time cost, the scratch conditions were set as 100 m/s (scratch speed), 2 nm (scratch depth) and 10 nm (scratch length). Furthermore, in the simulation, a microcanonical ensemble was used, and the time step was 1 fs. While, based on the established VS simulation model, the amplitude and frequency were set at 3 nm and 20 GHz, respectively; that is, the vibration was performed for 2 cycles within a scratch distance of 10 nm.

In order to verify the effectiveness of nano scale scratch simulation results, scholars usually compare the nano indentation/scratch experimental results with the molecular dynamics simulation results (Tian et al., 2020; Ikeshima et al., 2019). To verify the accuracy of the model, the same cutting depth simulation model were built with Tian et al. (2020). Tian et al., 2020 compared the indentation morphology with the TEM experiment results (Meng et al., 2016), and explained the accuracy of the model through the same phenomenon. From Fig. 3(a), it can be found that the force of 4 H-SiC was greater than 6 H-SiC, and then according to the comparison of Fig. 3. (c) and (d), it can be found that the magnitude and trend of the force are the almost same as those of Tian et al. (2020).

3. Results

In the scratch process of SiC with two abrasive grains, the coupling between adjacent abrasive grains on the workpiece were studied using the MD method. Consequently, the differences in scratch force, stress, surface morphology and influenced area volume between the CS and VS were compared. In addition, the effects of different scratch modes and different abrasive grains spacing d on the scratch process were also compared.

3.1. Scratch force

The scratch force must be analyzed to reflect the influence of various factors on the scratch process. In the MD simulation of abrasive grains scratch, the tangential, lateral and normal forces were defined as the vector sum of the X, Y and Z components of the force exerted by the workpiece atoms by the abrasive grain atoms (Shimizu et al., 2006).

3.1.1. Simultaneous scratch

During the simultaneous scratch, because the two abrasive grains moved simultaneously and the force conditions were the same, the scratch force of one abrasive grain can be analyzed, as shown in Fig. 4 (a). The abrasive grain spacing d was set to 6 nm, and the relationship between the force and displacement was analyzed. With an increase in

the scratch distance in CS, the tangential force and normal force first increased and then tended to be stable, while the lateral force was almost zero. In contrast, in the VS, with an increase in the scratch distance, the scratch force first increased and then fluctuated regularly with the movement of the abrasive grain trajectory. Further, compared with CS, the tangential force and normal force of VS were smaller than those of CS, while the lateral force was larger.

At different spacing d , the average scratch force of the stable stage (i. e., 5–10 nm) was calculated, as shown in Fig. 4(b). Among them, the calculation method of the average value of lateral force was special. Because the lateral force was affected by the trajectory, the change of lateral force was positive and negative alternately. And the positive and negative represents the direction of force, so the absolute values were calculated first and then the average values were calculated. Compared with a single abrasive grain scratch process, the scratch force of two abrasive grains with simultaneous scratches was smaller, and the degree of reduction was related to d . In the CS, the tangential and normal forces was observed to increase with an increase in d , and finally approach the tangential and normal forces of a single abrasive grain, while the lateral force was close to zero as the single abrasive grain. In contrast, in VS, with an increase in d , the tangential force exhibited almost no change, which was almost the same as that of a single abrasive grain scratched, while the normal and lateral forces increased gradually, which was close to the normal force of a single abrasive grain scratched.

3.1.2. Sequential scratch

In the process of sequential scratch, force analysis is required as two abrasive grains pass through the workpiece in sequence and the force of the second abrasive grain is the focus of the analysis. As shown in Fig. 5 (a) and (b), the abrasive grain spacing d is considered as 6 nm, and the relationship between force and displacement is analyzed. In the CS, after the first abrasive grain scratched, the scratch of the second abrasive grain becomes easier, thus the tangential and normal forces of the second abrasive grain were lower than those of the first abrasive grain, while the lateral force increased slightly. This is because the first abrasive grain produces a certain amount of atomic accumulation on both sides of the scratch trajectory. In the VS, the scratch force of the second abrasive grain was smaller than that of the first abrasive grain. When two abrasive grains scratched in phase, the scratch force of the second abrasive grain decreased significantly in the range of 0–2.5 and 5.0–7.5 nm. However, if scratched reverse, it decreased in the range of 2.5–5.0 and 7.5–10 nm.

At different spacing d , the average scratch force of the stable stage (i. e., 5–10 nm) was calculated, as shown in Fig. 5(c). The scratch process of the first abrasive was actually a single abrasive scratch process, thus, the scratch force of the first abrasive remained unchanged with d . It can be observed that the tangential and normal forces gradually increase with d . In the CS, when d reached 8 nm, the tangential and normal forces were almost the same as those of the first abrasive grain. Further,

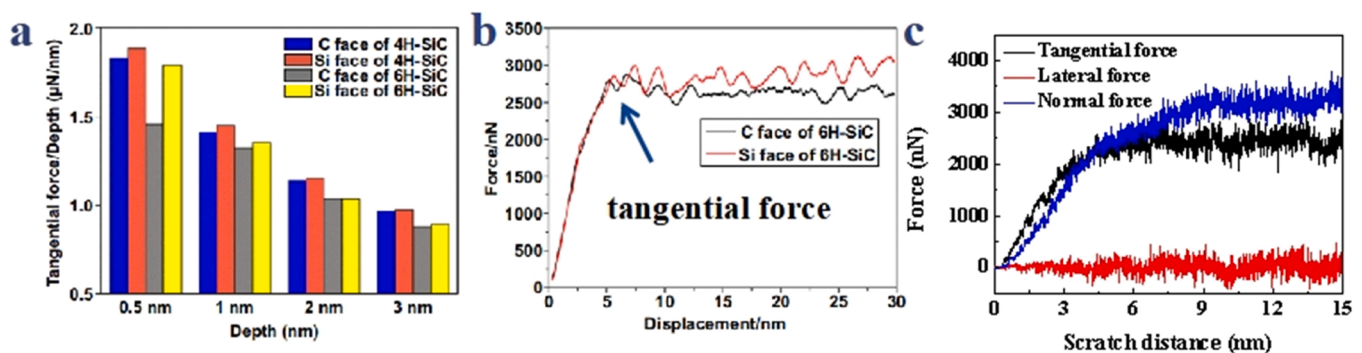


Fig. 3. (a) Comparison of tangential force of 4 H-SiC and 6 H-SiC at different cutting depths, (b) the change trend of tangential force when the cutting depth was 3, and (c) in this paper, the variation trend of scratch force when the cutting depth of the model was 3.

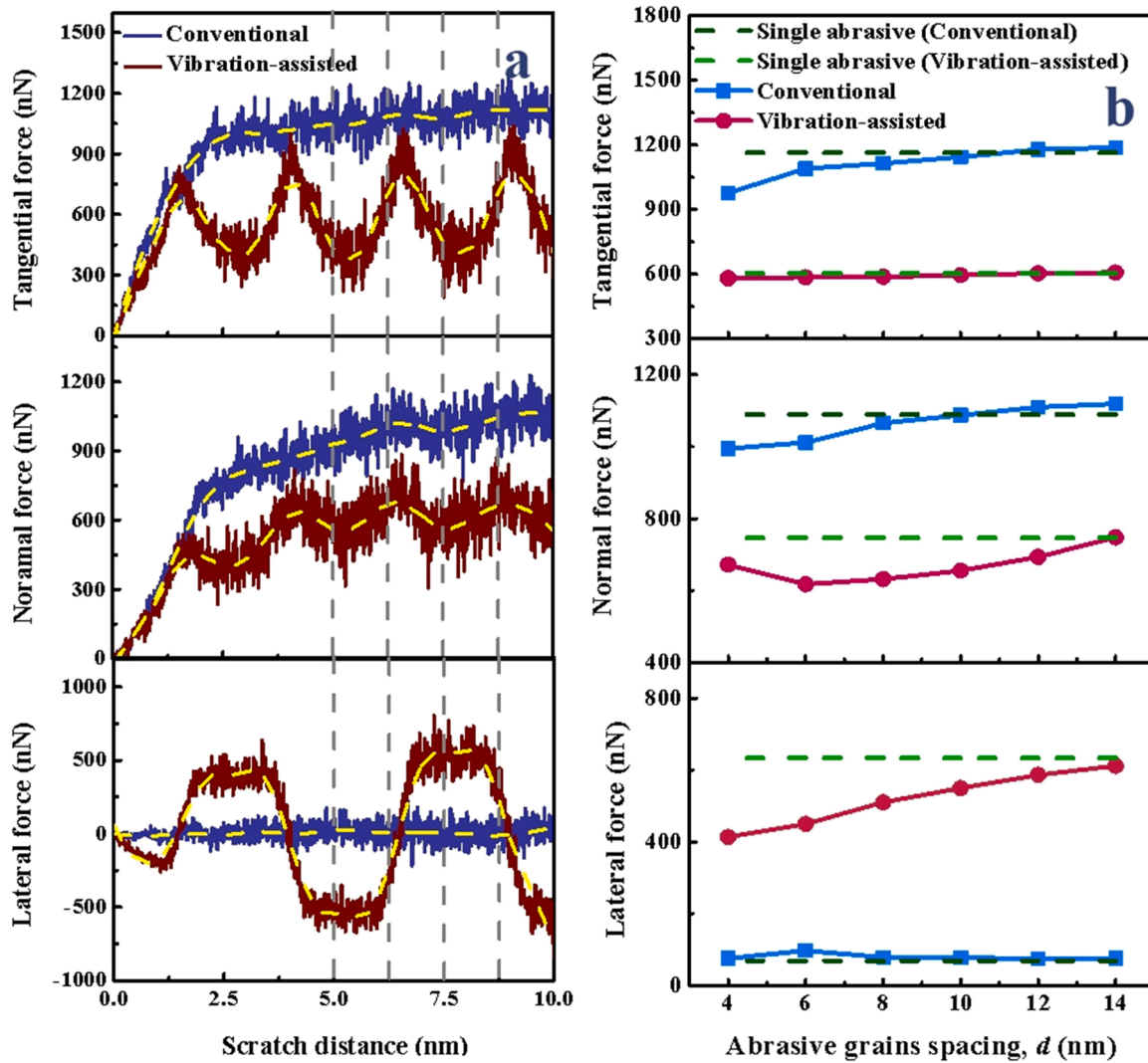


Fig. 4. (a) Scratch force at the $d = 6$ nm when the abrasive grains scratched simultaneously and (b) Comparison of scratch force at different spacing when the abrasive grains scratched simultaneously.

because of the accumulation of abrasive grains on both sides of the track after the first abrasive grain was scratched, the lateral force of the second abrasive grain increased significantly when d was greater than 2 nm. With an increase in d , the influence of the accumulated atoms on the scratch of the second abrasive grain decreased gradually, and the lateral force gradually decreased to nearly zero. However, in the VS, the tangential and normal forces were smaller than those of the CS, while the lateral force was larger. In addition, the scratch force of the second abrasive grain increased gradually with an increase in d , and approached the scratch force of the first abrasive grain. When d reached 14 nm, the scratch force of the second abrasive grain was the same as that of the first abrasive grain. Furthermore, under most conditions, the scratch force of the second abrasive grain in the vibration-assisted reversed scratch was slightly larger than that of the vibration-assisted in-phase scratch, and the difference was not significant.

3.2. Von-Mises stress

During machining, stress is the primary cause of workpiece damage. Therefore, the stress distribution on the workpiece surface during scratching must be analyzed, and the difference in stress size and stress distribution between CS and VS needs to be compared. The von-Mises stress distribution on the workpiece surface caused by abrasive grains

during scratching can be obtained using the MD software. The principle involves calculating the stress components δ_{xx} , δ_{yy} , δ_{zz} , δ_{xy} , δ_{xz} , and δ_{yz} of the atom. The Von-Mises stress can be expressed as (Chavoshi and Luo, 2016b):

$$\sigma_{\text{von}} = \sqrt{3(\sigma_{xy}^2 + \sigma_{xz}^2 + \sigma_{yz}^2)} \frac{1}{2} [(\sigma_{xx} - \sigma_{yy})^2 + (\sigma_{xx} - \sigma_{zz})^2 + (\sigma_{zz} - \sigma_{yy})^2]$$

In the process of VS, the direction of the stress concentration area would constantly change with the change of abrasive grain trajectory, and the change of stress is also related to abrasive grain trajectory (Chen, 2021). In this paper, the stress at the scratch distance of 10 nm would be selected for comparison.

3.2.1. Simultaneous scratch

In the two abrasive grains scratched simultaneously, the stress distribution nephogram at $d = 6$ nm was used to analyze the stress distribution in the CS and VS. The section was made along the center line of the abrasive grains to observe the stress distribution between abrasive grains, as shown in Fig. 6. The top view of the stress distribution nephogram is shown in Fig. 7(a). In the CS, the area with larger stress was larger than that of the VS, which was primarily concentrated at the front and below the two abrasive grains. Further, the direction of the stress concentration was closely related to the direction of movement of

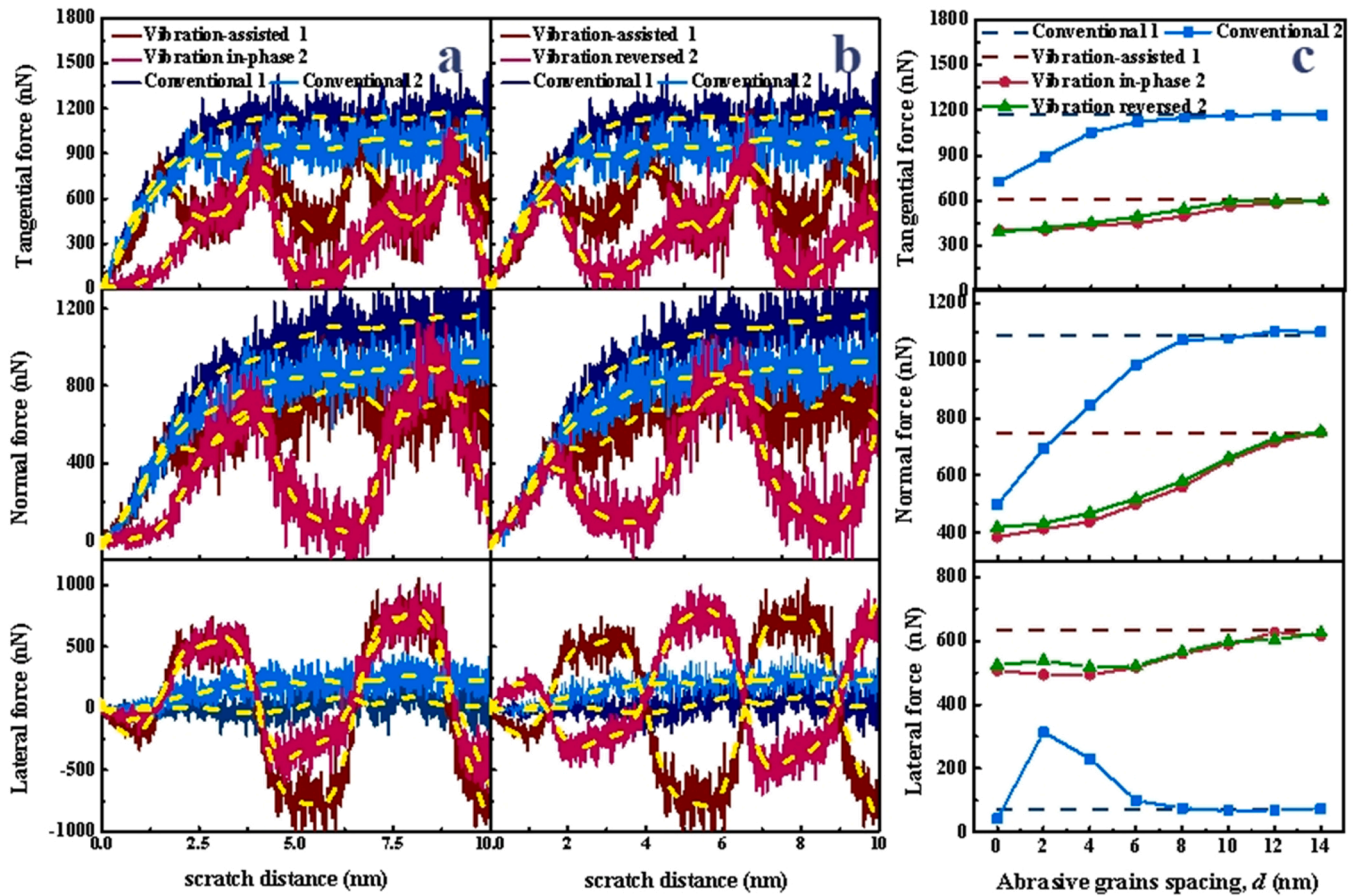


Fig. 5. Comparison of the scratch force at the $d = 6$ nm when the abrasive grains scratched sequentially between the (a) CS and vibration in-phase scratch and (b) CS and vibration reversed scratch. (c) comparison of scratch force at different spacing when the abrasive grains scratched sequentially.

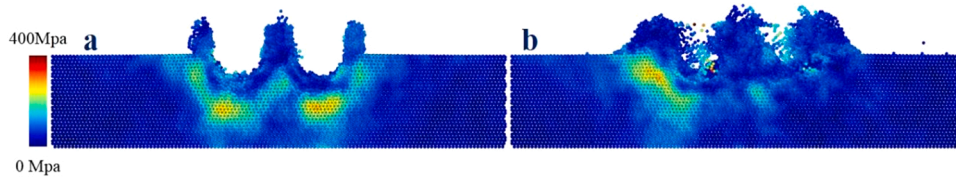


Fig. 6. Comparison of the stress at the $d = 6$ nm when the abrasive grains scratched simultaneously between the (a) CS and (b) VS.

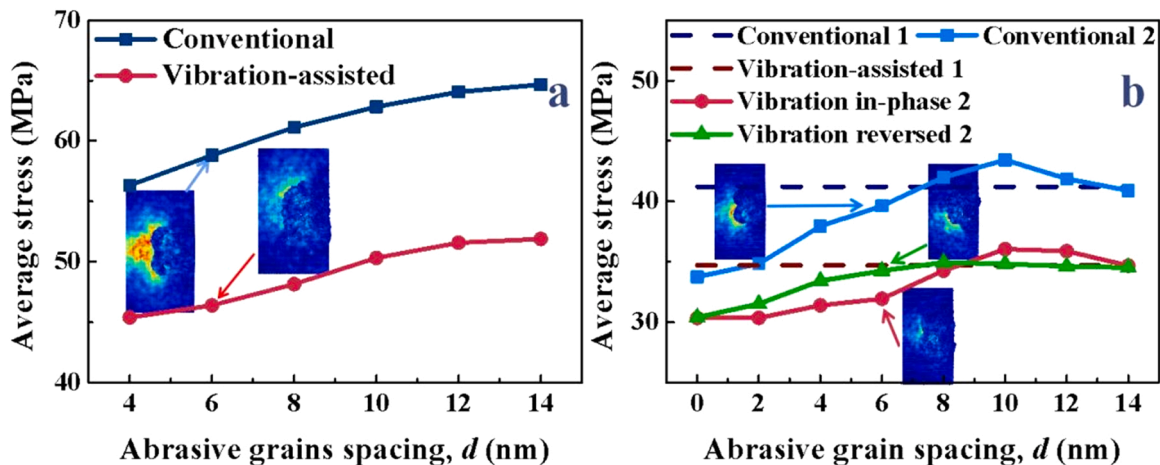


Fig. 7. Comparison of the average stress at different d when the abrasive grains scratched (a) simultaneously and (b) sequentially.

the abrasive grains. However, compared with CS, the stress of VS reduced, and the direction of stress concentration was diagonally forward and diagonally below.

To compare the change in stress under different abrasive grain spacing d in the process of simultaneous scratch, the stress values of each atom in the model were averaged, and the results are shown in Fig. 7(a). It is evident that the average stress increased with an increase in d , regardless of CS or VS. Moreover, comparing CS and VS, the average stress of the latter was significantly lower than that of the former, and the stress concentration area was significantly smaller than that of CS.

3.2.2. Sequential scratch

In the two abrasive grains scratched separately, the stress distribution nephogram of two abrasive grains scratched at 10 nm when $d = 6$ nm was used to analyze the stress distribution in the process of CS and VS. The section was made along the center line of the abrasive grains to observe the stress distribution between abrasive grains, as shown in Fig. 8. The top view of the stress distribution nephogram is shown in Fig. 7(b). Because the abrasive grains scratched sequentially, the stress was primarily concentrated around the currently moving abrasive grains. In the CS, the area with the larger stress was larger than that of the VS, and the stress concentration was primarily at the front and below the abrasive grains. In contrast, the stress of VS was lower, and the stress concentration was in the same direction as the velocity, which was diagonally forward and diagonally below the abrasive grain.

To compare the change in stress under different spacings in the process of separate scratching, the stress values of each atom in the model were averaged, and the results are shown in Fig. 7(b). It can be observed that the average stress value of the second abrasive grain increased with an increase in d and gradually approached the stress value of the first abrasive grain. Further, the stress concentration area of VS was obviously smaller than that of CS and the average stress of VS was lower than that of the CS. Moreover, for d values smaller than 10 nm, the stress of the second abrasive grain during vibration-reversed scratching was slightly greater than that during in-phase scratching.

3.3. Surface morphology

The surface machining quality and material removal were analyzed by studying the surface morphology. Further, through the study of the

atomic displacement, the movement of atoms in the machining process was observed, and the coupling of two abrasive grains in the machining process could also be observed conveniently.

3.3.1. Simultaneous scratch

In the process of two abrasive grains scratching simultaneously, the surface morphologies of CS and VS under different abrasive grain spacings d were compared, as shown in Fig. 9. In the CS, the movement of the atoms between the two abrasive grains in the Y-direction was not obvious. When d reached 8 nm, the scratches of the two abrasive grains were almost independent. However, in VS, more atoms were removed and those between the two abrasive grains moved violently in the Y-direction. When d reached 12 nm, the scratches of the two abrasive grains were not completely separated. Thus, compared with the CS, the influence area of VS was significantly greater than that of CS, and the influence of the two abrasive grains was intensified by vibration. Furthermore, in the VS, the independent abrasive grain spacing (14 nm) of the scratch marks was significantly larger than that of the CS (8 nm).

3.3.2. Sequential scratch

The surface morphologies of the two abrasive grains in the scratch process were compared under different abrasive grain spacing d , as shown in Fig. 10. In the CS, the second abrasive grain squeezed the atoms between the two abrasive grains in the direction of the first abrasive grain and when d reached 8 nm, the scratches of the two abrasive grains were almost independent. However, in the VS, more atoms were removed and those between the two abrasive grains moved violently in the Y-direction. Further, when d reached 14 nm, the scratches of the two abrasive grains were completely separated. Thus, compared with the CS, the scratched area of VS was obviously, and the maximum width of the scratched area of the vibration-reversed scratch was larger than that of the in-phase scratch, which was related to the trajectory. Moreover, in the VS, the independent abrasive grain spacing (14 nm) of the scratch marks was significantly larger than that of CS (8 nm).

3.4. Machining influenced material

In the scratch, the crystal structure of the material on the surface of the workpiece changed owing to the stress of the abrasive grains. When

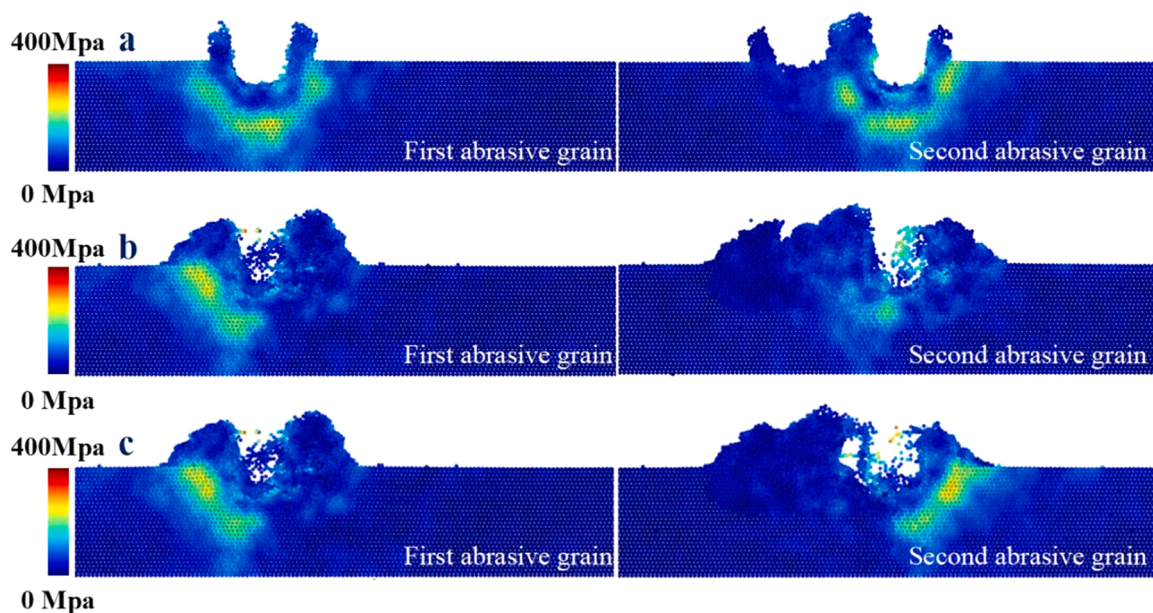


Fig. 8. Comparison of the stress at the $d = 6$ nm when the abrasive grains scratched sequentially between the (a) CS, (b) vibration in-phase scratch and (c) vibration reversed scratch.

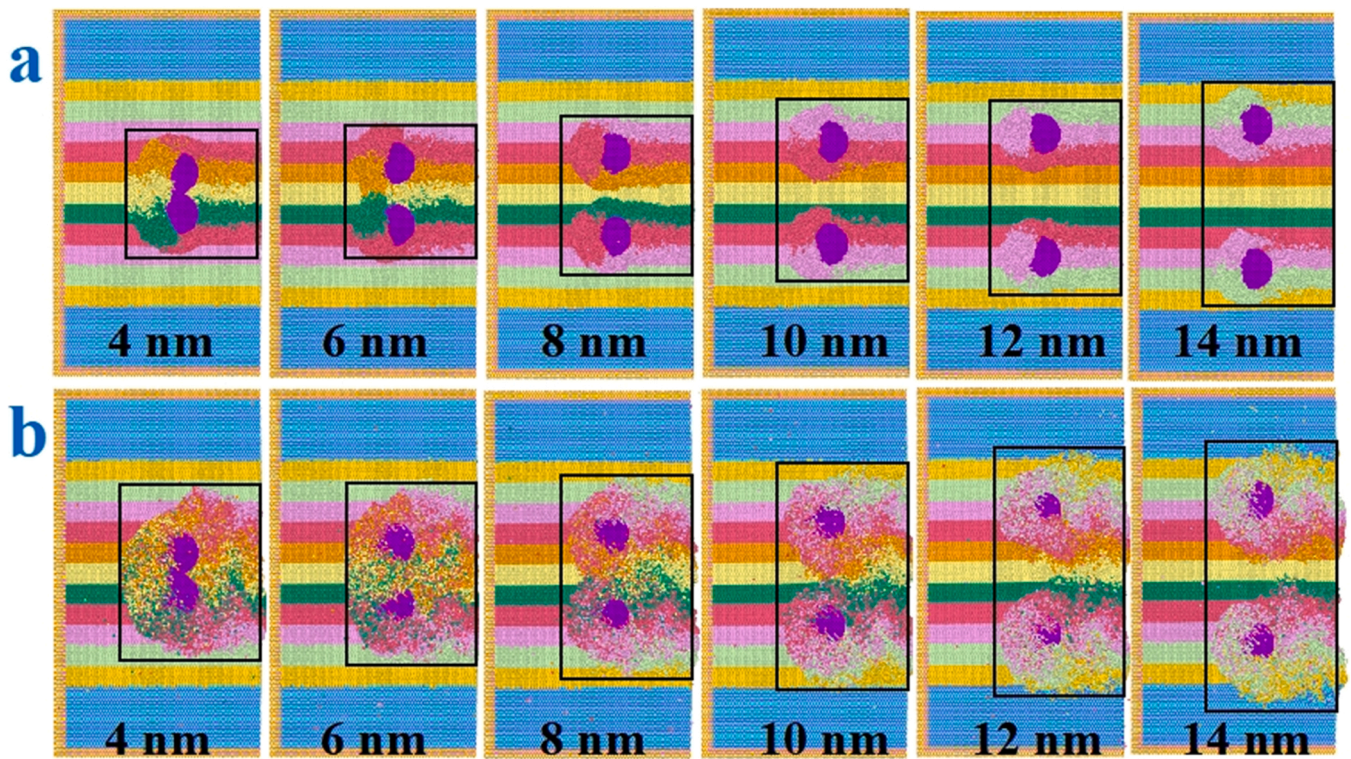


Fig. 9. Comparison of the surface morphology and atomic displacement on the surface in the (a) CS and (b) vibration-assisted simultaneous scratch at different abrasive grains spacing d , where the black boxes represent the scratched surface area and the width of each colored layer along the Y-direction was 2 nm.

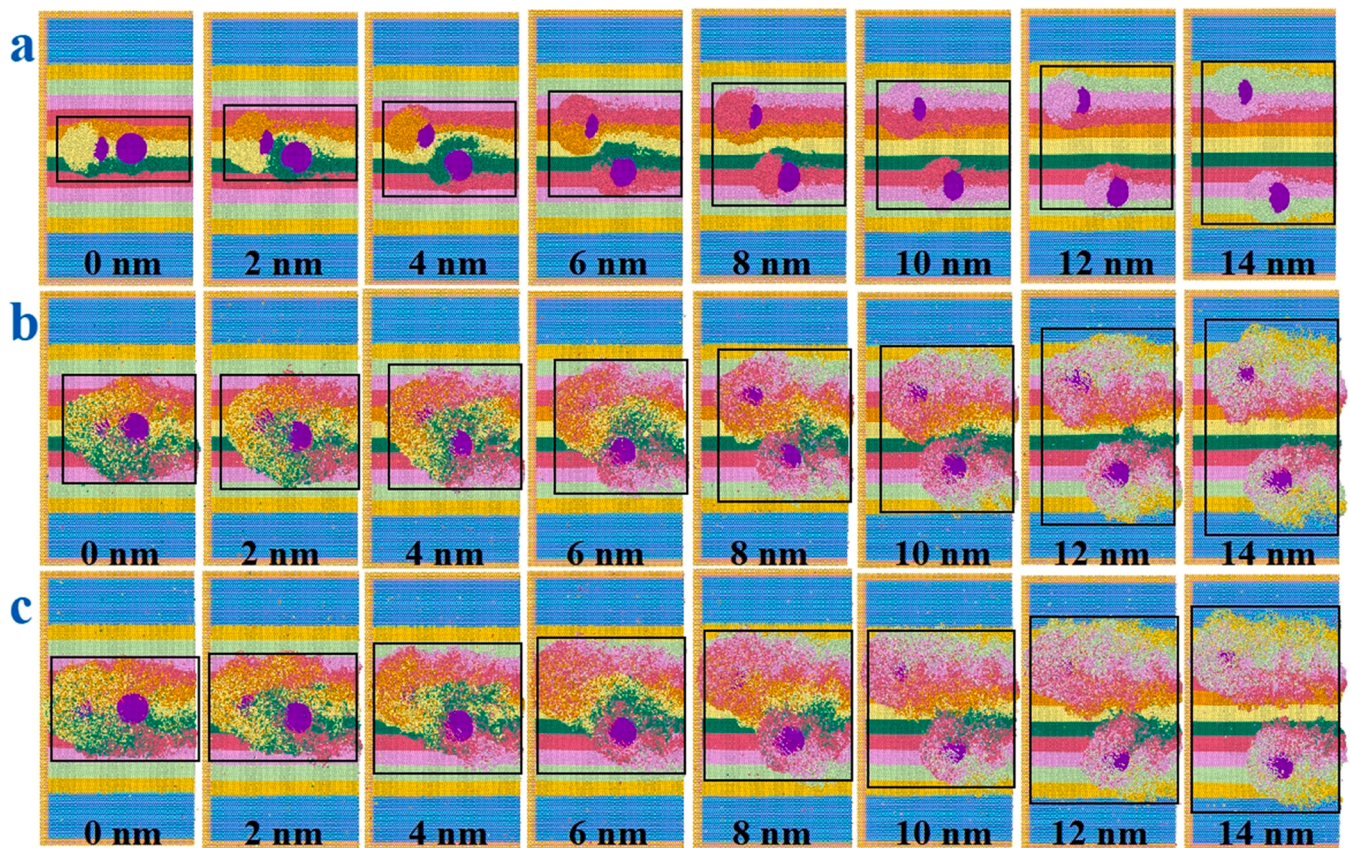


Fig. 10. Comparison of the surface morphology and atomic displacement on the surface in the (a) CS, (b) vibration in-phase and (c) vibration reversed sequential scratch at different abrasive grains spacing d , where the black boxes represent the scratched surface area and the width of each colored layer along the Y-direction was 2 nm.

the abrasive grains machine the workpiece, it will destroy the original perfect lattice structure and produce phase transformation, resulting in amorphous regions (Lu et al., 2019), which can be interpreted as the machining influenced material of abrasive grains. This formation can reflect the machining effect in the scratch process (Meng et al., 2016), and to a certain extent, it will form subsurface damage (Lin et al., 2021). In the MD simulation of the double abrasive grain scratch process, the identify diamond structure module in OVITO can be used to analyze the crystal structure.

3.4.1. Simultaneous scratch

As shown in Fig. 11(a), when d was 6 nm, the situation of the amorphous layer in the scratch was compared. In CS, the bottom of the amorphous layer had two obvious grain profiles and some fluctuations. Compared with the CS, the thickness D (Z direction) of the amorphous layer was smaller, the width (Y direction) was wider, and the morphology of the bottom of the amorphous layer was smoother, almost in a straight line, which can be explained to a certain extent by the fact that in the process of VS, the machining influenced material area was larger and the surface quality was better.

The machining volumes were calculated based on the number of amorphous atoms. The calculation formula is as follows:

$$V = \frac{N_a}{N_m} \times V_m$$

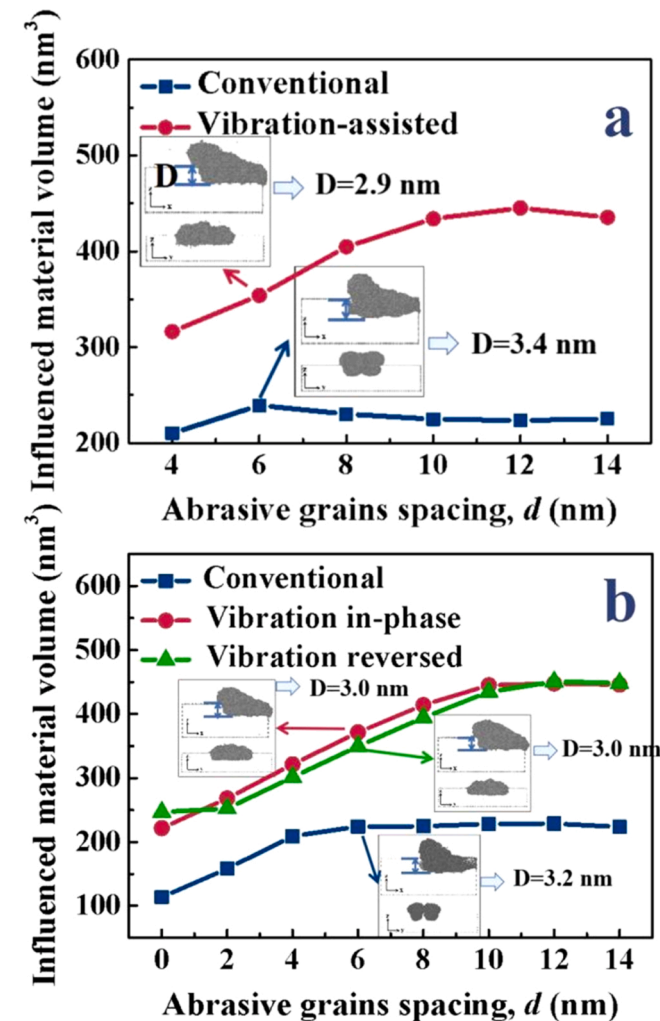


Fig. 11. Volume comparison of machining influenced material with different abrasive grain spacing d when the abrasive grains scratched (a) simultaneously and (b) sequentially.

where N_a and N_m are the numbers of atoms in the amorphous layer and the workpiece, respectively, and V_m is the volume of the workpiece. The calculation results are shown in Fig. 11(a). With an increase in d , the influenced material volume gradually increased. In the CS, when d was greater than 6 nm, the machining volume remained stable and did not increase. Whereas, in the VS, when d reached 12 nm, the influenced material volume increased slightly.

3.4.2. Sequential scratch

As shown in Fig. 11(b), when d was 6 nm, the amorphous layer in the process of sequential scratching was compared. Herein, the morphology of the machining-influenced material obtained by sequential scratch and simultaneous scratch was very similar. Further, the influenced material volume was larger, and the surface quality was better in the VS process. The vibration-assisted scratch effectively reduced the thickness of amorphous layer, and the thickness of amorphous layer is almost the same for vibration in-phase scratch and vibration reversed scratch.

The volume of the machining influenced material was calculated according to the number of amorphous atoms. As shown in Fig. 11(b), with an increase in d , the volume of the machining influenced material increased gradually. In the CS, when d was greater than 6 nm, the volume of the influenced material remained unchanged. However, in the VS, when d reached 12 nm, the volume of the influenced material increased slightly and tended to be flat. Except for $d = 0$ nm, the volume of the machining influenced material of the vibration-reversed scratch was slightly larger than that of the vibration in-phase scratch. Further, the morphology of influenced material area after machining also showed obvious differences. With the application of vibration, the width of the influence area was wider, and the morphology of the influence area between two abrasive grains was smoother than that of CS.

Whether scratch simultaneously or sequentially, it is evident that owing to the application of vibration, the mutual influence between abrasive grains enhanced, and the surface morphology after machining also showed obvious differences. When vibration was not applied, the surface scratches possessed obvious directionality, showing obvious scratch morphology. Following the application of vibration, obvious scratches were not observed on the surface, and the surface was relatively smoother.

4. Discussions

The essence of grinding is the comprehensive effect of sliding, plowing, and cutting on the workpiece surface by a great number of discrete abrasive grains distributed on the grinding wheel. The different situations of abrasive grains in the actual machining process were simulated by setting two abrasive grains to scratch the workpiece simultaneously and sequential.

When two abrasive grains scratched the workpiece simultaneously, the scratch force and stress of the two abrasive grains were almost identical and changed synchronously. Owing to the coupling between the two abrasive grains, the scratch force and stress of the two abrasive grains were smaller than those of the single abrasive grain in CS. Consequently, by calculating the force reduction ratio of a simultaneous scratch compared to that of a single abrasive grain scratch in CS, the effects of applying vibrations were studied during the simultaneous scratch. The calculation formula is as follows:

$$\text{Force reduction ratio of simultaneous scratch} = \frac{F_1 - F}{F_1} \times 100\%$$

where F is the scratch forces during simultaneous scratching and F_1 is the single-abrasive-grain scratching in CS. The calculation results are shown in Fig. 12(a). With increase in the spacing between abrasive grains, the reduction ratio gradually decreased. In the process of VS, the force reduction ratios were significantly higher than that of CS. Therefore, the application of vibration had a more significant impact on the

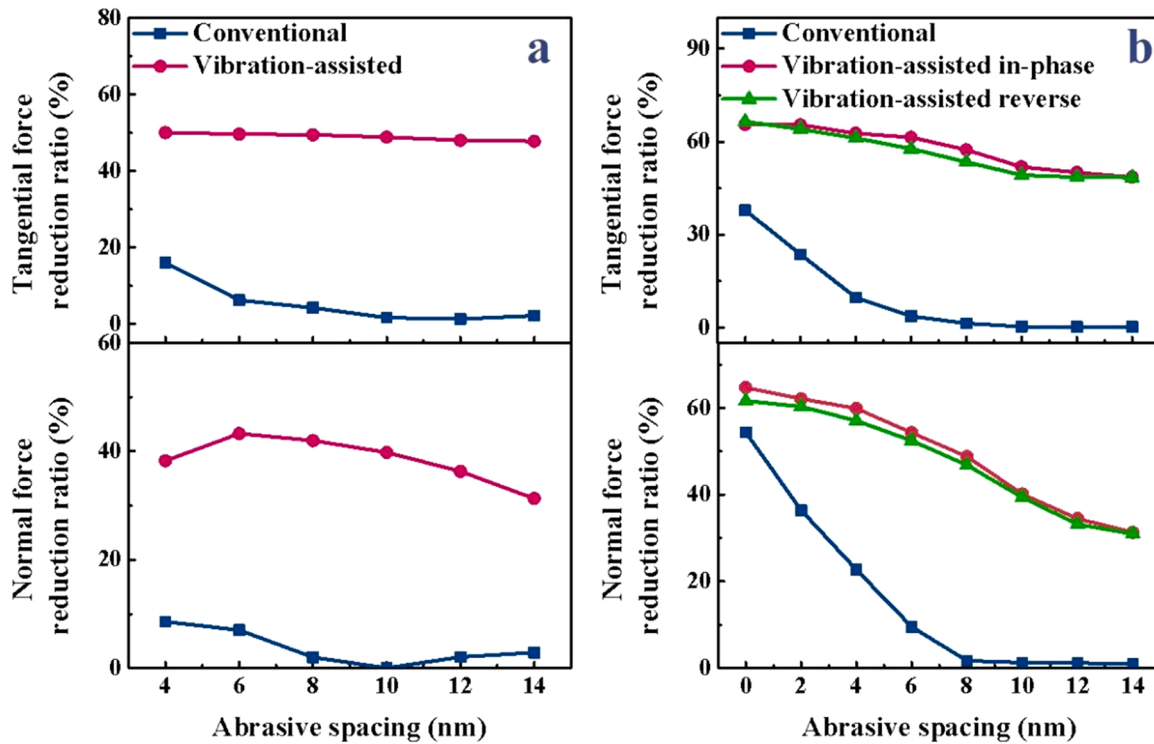


Fig. 12. (a) In simultaneous scratch process, the reduction ratios between the scratch force and the scratch force of a single abrasive grain in conventional scratch were compared. (b) In sequential scratch process, the reduction ratios between the scratch force and the scratch force of a single abrasive grain in conventional scratch were compared.

reduction of the force. In the CS, the scratch force was smaller than that of the single abrasive, and the stress concentration area was between the two abrasive grains. Further, because the scratch trajectories were straight, the scratch directions were obvious in the scratch process, although the flatness of the machined surface area was poor, with an obvious bulge. In contrast, in the VS, the distribution of the scratch force was more uniform, and the anisotropy of the scratch force increased, such that the stress decreased significantly. In addition, the stress concentrated along the motion direction of the abrasive grains, and the surface roughness of the machined surface was better. Upon analyzing the influence of d on the simultaneous scratch according to the changes in the scratch force, scratched surface, and volume of the machining-influenced material, the VS was found to intensify the coupling between the two abrasive grains.

When two abrasive grains scratched the workpiece separately, because the scratch of the first abrasive grain was equivalent to that of a single abrasive grain, the second abrasive grain, and the influence of the scratch of the first abrasive grain on the scratch of the second abrasive grain were studied in detail. The force reduction ratio was calculated as follows:

$$\text{Force reduction ratio of sequential scratch} = \frac{F_1 - F_2}{F_1} \times 100\%$$

where F_2 is the scratch forces of the second abrasive grains during sequential scratching and F_1 is the single-abrasive-grain scratching in CS. The calculation results are presented in Fig. 12(b). Because of the first abrasive grain scratching, the scratch difficulty of the second abrasive grain was lower, and the surface material of the workpiece was easier to remove. In the VS, the scratch force of the second abrasive grain was significantly lower than that of the first abrasive grain. At the same time, compared with the CS of single abrasive grain, the reduction ratio of scratch force was significantly great. Further, the stress was concentrated at the front of the second abrasive grain. The scratch trajectory fluctuated, and the thickness of the machining-influenced material

region was smaller; that is, the damage was smaller. Simultaneously, the volume of the machining influence area was large, and the quality of the machined surface was good and flat. When studying the influence of d on the sequential scratch process, the scratch force reduction ratio, surface morphology, and machining influenced the material volume, it was found that the scratch force reduction ratio of the VS was significantly larger than that of the CS. Further, there was no obvious difference in the vibration in-phase scratch and vibration reversed scratch. Moreover, when scratching sequentially, there was a critical abrasive grain spacing d_{max} , which resulted in the volume of the influenced material reaching the maximum. When d reached d_{max} , it was almost twice that of a single abrasive. In addition, the scratch force tended to the scratch force of single abrasive grain, and the stress did not change significantly with an increase in d . Furthermore, the scratch of the first abrasive grain did not influence the scratch process of the second abrasive grain.

To compare the coupling between abrasive grains more intuitively, a new evaluation index, the volume overlap ratio of the influenced material region (r) was proposed, which can measure the degree of coupling effect between abrasive grains. It was defined by the overlap degree of the volume of the influenced material of two abrasive grains. The calculation formula is as follows:

$$r = \frac{|V_s \times 2 - V|}{V_s} \times 100\%$$

where V_s is the machining influenced material volume of a single abrasive grain scratch. The larger r is, the greater is the intersection between the two abrasive grain trajectories, and the stronger are the coupling. The smaller the value of r , the smaller the overlap area of the two abrasive grains. For sufficiently large distance between the abrasive grains, the volume of the influence area was almost twice that of a single abrasive grain. Further, a critical spacing d_{max} maximized the volume of the influence area. When r was zero, no intersection between the scratch tracks of the two abrasive grains were observed, and the scratch process of the two abrasive grains no longer influenced each other. As shown in

Fig. 13(a), during the simultaneous scratch process, when the spacing between the abrasive grains was small, r was large. However, as the distance between the abrasive grains increased, the coupling between them gradually decreased and finally approached zero. Moreover, compared with CS, the overlap ratio of VS was greater, and the d_{max} of VS was also greater than that of CS.

As shown in Fig. 13(b), during the sequential VS, the influence of the first abrasive scratch on the second one was significantly greater than that during CS, and d_{max} was also significantly greater than that during CS. When d was 0, the r of the CS and the vibration in-phase scratch were 100%. Herein, the reduction ratios of the scratch force of the CS and the vibration in-phase scratch were relatively large. Further, for d values greater than 0 nm, r decreased gradually with an increase in d . In the CS, r was far less than that of the VS, thus, the scratch force decreased much less than that of the CS. The results showed that the larger the volume overlap between the influence areas of the two abrasive grains, the larger the area machined by the second abrasive grain had been machined by the first abrasive grain, and thus, the greater the reduction in the scratch force. Therefore, r can reflect the coupling between the abrasive grains to a certain extent.

Combined with the stress distribution and the size of the machining influenced area, whether scratching was simultaneous or sequential, in the CS, the location where stress was greater was directly below the abrasive grains and the front side of the abrasive grains. In the VS, for the influence of the direction of movement, the place where the stress was greater was found to be below the abrasive grain side and diagonally in front of the abrasive grain. During VS, the depth of the machining influenced area was shallower, but the width was wider. Therefore, the depth of subsurface damage can be effectively suppressed; however, the width of the machining area is enlarged and effectively improves the processing efficiency.

By studying the relationship between the overlap ratio and the force reduction ratio, it can be found that VS significantly increased the force reduction ratio. Further, as can be seen in the Fig. 14(a), in the process of simultaneous scratch, the application of vibration significantly improved the overlap ratio. At the same time, in the process of CS, with the increase of overlap ratio, the force reduction ratio gradually increased. In the VS, the change of reduction proportion was not significant with the increase of overlap ratio. As can be seen in the Fig. 14 (b), in the process of sequential scratch, the force reduction ratio increased obviously with the increase of overlap ratio. And the reduction ratio of VS was significantly greater than that of CS.

According to previous studies [26], the anisotropy factor can be used to evaluate the uniformity of scratch force distribution. As shown in Fig. 15 (a), in the process of simultaneous scratch, with the increase of the overlap ratio, the change of the anisotropy factor of CS was not

obvious, and the anisotropy factor in the VS increased slightly. It showed that in the simultaneous scratch, the overlap ratio of the movement of abrasive grains increased, which was conducive to the uniform distribution of scratch force, so as to reduce stress and damage depth. In the process of sequential scratch, as shown in Fig. 15(b), whether CS or VS, with the increase of overlap ratio, the anisotropy factor first decreased and then increased. This result showed that there was an optimal overlap ratio in the sequential scratch, which can make the scratch force distribute most uniform.

In the actual grinding process, due to the positional relationship between abrasive grains, the sequential scratches are dominant. Considering that in the actual machining process, there were far more than two abrasive grains on the grinding wheel, the scratch movements of multiple abrasive grains were simulated using MATLAB to observe the surface quality of the scratch when multiple abrasive grains were scratched. The simulation conditions were as follows: Five abrasive grains radius as 2 nm and lateral distance between two abrasive grains of 4 nm. The material removal and surface quality of scratch process were calculated as shown in Fig. 16. It is evident that after CS, the surface scratches are obvious and have directionality. In contrast, during VS, owing to the vibration of abrasive grains, the scratched area was significantly larger than that of CS, the surface was more uniform, and the surface flatness was much better than that of CS. Compared with vibration reversed scratch, vibration in-phase scratch had better machining quality, but the machined area was smaller.

Therefore, it is evident that owing to the application of vibration, the overlap ratio increased and the anisotropy factor decreased significantly. And the directionality of the scratched surface wear marks significantly were weakened, the anisotropy enhanced, and the surface roughness reduced. Further, the mutual influence between abrasive grains enhanced. Thus, the simulation results can provide significant guidance for the design of the abrasive grain arrangement on the grinding wheel, the optimal overlap ratio of abrasive grains machining area can be obtained, and the optimal machining effect can be obtained.

5. Conclusions

The coupling mechanism of abrasive grains in a double-grain model have investigated using molecular dynamics simulations. Various scratch modes have been examined. The differences between the conventional scratch (CS) and vibration-assisted scratch (VS) were compared and analyzed based on the scratch force, stress distribution, surface morphology and influenced material volume. The coupling improves the grinding efficiency and workpiece surface quality. More conclusions are follows.

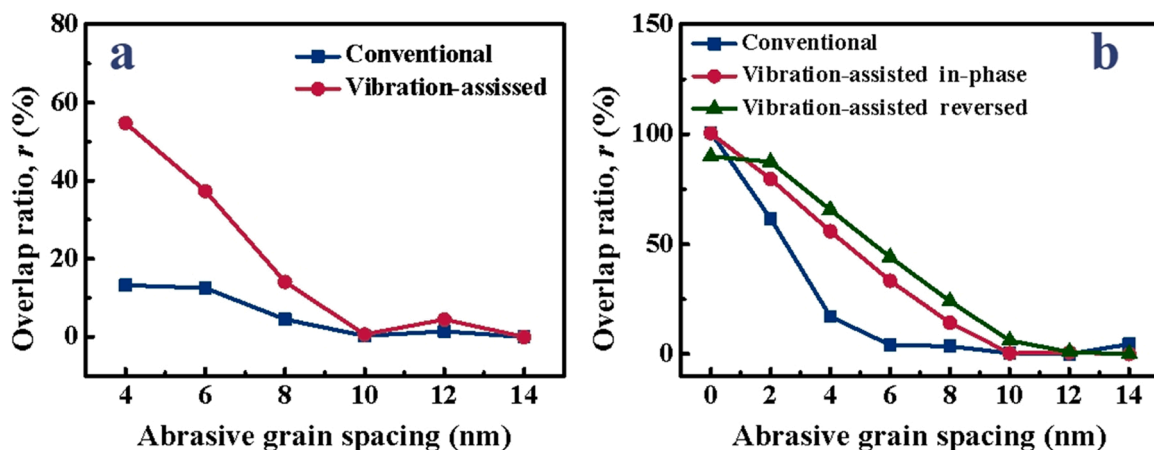


Fig. 13. Comparison of overlap ratio of machining influenced material between conventional and vibration-assisted scratch in (a) simultaneous scratch and (b) sequential scratch.

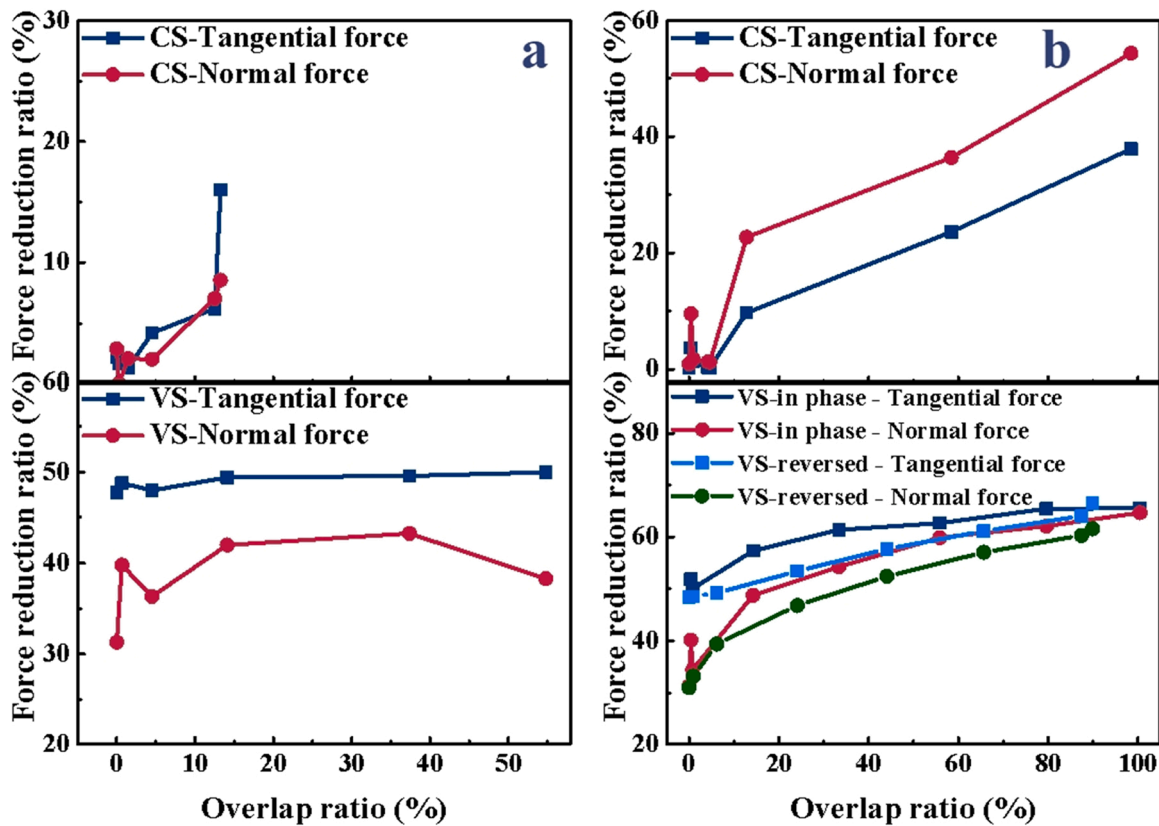


Fig. 14. In the conventional scratch and vibration-assisted scratch processes, the relationship between the overlap ratio and force reduction ratio in (a) simultaneous scratch and (b) sequential scratch were compared.

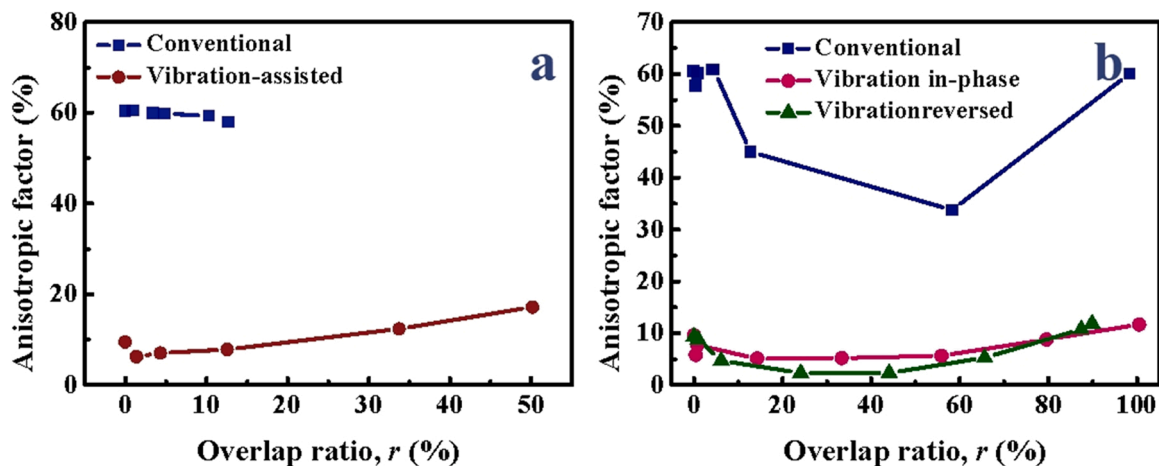


Fig. 15. In the conventional scratch and vibration-assisted scratch processes, the relationship between the overlap ratio and anisotropic factor in (a) simultaneous scratch and (b) sequential scratch were compared.

- (1) The increased coupling between abrasive grains improved the surface quality and reduced the force. The applied of vibration can effectively intensify the coupling between the different abrasive grains. In the VS, the critical spacing of the inhibition of the coupling between abrasive grains increased obviously.
- (2) The overlap ratio can reflect the degree of the coupling. The greater the overlap ratio, the more obvious the coupling between the abrasive grains, and the greater the impact on the scratch force and stress.
- (3) The application of vibration in the simultaneous scratch was conducive to increase the overlap ratio. The greater the overlap

- ratio, the force reduction ratio increased. In the sequential scratch, the larger the overlap ratio was, the lower the force was, and the anisotropic factor decreased first and then increased, and there was a minimum value, so as to achieve the optimal effect.
- (4) VS changed the stress distribution, effectively reduced the range of the area with large stress and the anisotropy factor, such that the thickness of the machining influenced area reduced, width increased, processing efficiency improved. And VS can enhance the anisotropy of the scratched surface, reduce the scratch force and surface roughness, and facilitate subsequent machining.

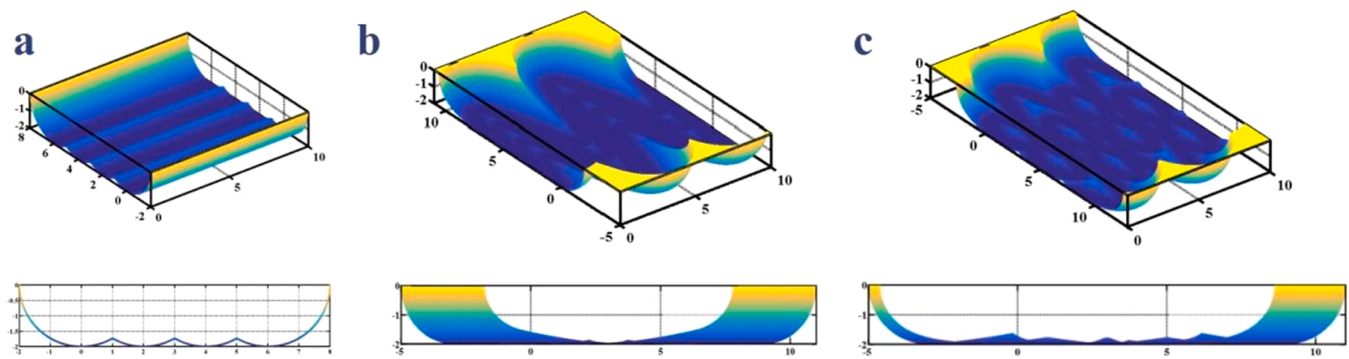


Fig. 16. MATLAB simulation diagram of multiple abrasive grains:(a) conventional, (b) vibration in-phase and (c) vibration reversed scratch.

Further research on the coupling mechanism between abrasive grains can guide the arrangement of abrasive grains in the grinding wheel and optimize the machining process.

Declaration of Competing Interest

The authors declare that they have no known competing financial interests or personal relationships that could have appeared to influence the work reported in this paper.

Acknowledgments

This work was supported by the National Natural Science Foundation of China (Grant Nos. 52175404, 51835004) and the State Key Laboratory of Mechanical System and Vibration, China (Grant No. MSV202112). Q. P. would like to acknowledge the support provided by LiYing Program of the Institute of Mechanics, Chinese Academy of Sciences, China through Grant No. E1Z1011001.

References

- Baraheni, M., Amini, S., 2019. Predicting subsurface damage in silicon nitride ceramics subjected to rotary ultrasonic assisted face grinding. *Ceram. Int.* 45 (8), 10086–10096. <https://doi.org/10.1016/j.ceramint.2019.02.055>.
- Cai, L., Guo, X., Gao, S., Li, Z., Kang, R., 2019. Material removal mechanism and deformation characteristics of AlN ceramics under nanoscratching. *Ceram. Int.* 45 (16), 20545–20554. <https://doi.org/10.1016/j.ceramint.2019.07.034>.
- Cao, J., Wu, Y., Lu, D., Fujimoto, M., Nomura, M., 2014. Material removal behavior in ultrasonic-assisted scratching of SiC ceramics with a single diamond tool. *Int. J. Mach. Tools Manuf.* 79, 49–61. <https://doi.org/10.1016/j.ijmactools.2014.02.002>.
- Chavoshi, S.Z., Luo, X., 2016a. An atomistic simulation investigation on chip related phenomena in nanometric cutting of single crystal silicon at elevated temperatures. *Comput. Mater. Sci.* 113, 1–10. <https://doi.org/10.1016/j.commatsci.2015.11.027>.
- Chavoshi, S.Z., Luo, X., 2016b. Molecular dynamics simulation study of deformation mechanisms in 3C-SiC during nanometric cutting at elevated temperatures. *Mater. Sci. Eng. A* 654, 400–417. <https://doi.org/10.1016/j.msea.2015.11.100>.
- Chavoshi, S.Z., Xu, S., 2019. Nanoindentation/scratching at finite temperatures: Insights from atomistic-based modeling. *Prog. Mater. Sci.* 100, 1–20. <https://doi.org/10.1016/j.pmatsci.2018.09.002>.
- Chen, Y., Hu, Z., Jin, J., Li, L., Yu, Y., Peng, Q., Xu, X., 2021. Molecular dynamics simulations of scratching characteristics in vibration-assisted nano-scratch of single-crystal silicon. *Appl. Surf. Sci.* 551, 149451. <https://doi.org/10.1016/j.apsusc.2021.149451>.
- Dai, J., Su, H., Zhou, W., Zhang, Q., Zheng, Y., 2019. Experimental and numerical investigation on the interference of diamond grains in double-grain grinding silicon carbide ceramics. *J. Manuf. Process.* 44, 408–417. <https://doi.org/10.1016/j.jmapro.2019.06.014>.
- Duan, N., Yu, Y., Wang, W., Xu, X., 2017. Analysis of grit interference mechanisms for the double scratching of monocrystalline silicon carbide by coupling the FEM and SPH. *Int. J. Mach. Tools Manuf.* 120, 49–60. <https://doi.org/10.1016/j.ijmactools.2017.04.012>.
- Dulak, M., Thygesen, K.S., Norskov, J.K., 2011. Finite Size Effects in Chemical Bonding: From Small Clusters to Solids. *Catalysis Letters* 141 (8), 1067–1071. <https://doi.org/10.1007/s10562-011-0632-0>.
- Feng, J., Wan, Z., Wang, W., Ding, X., Tang, Y., 2019. Crack behaviors of optical glass BK7 during scratch tests under different tool apex angles. *Wear* 430, 299–308. <https://doi.org/10.1016/j.wear.2019.05.023>.
- Feng, J., Wan, Z., Wang, W., Huang, X., Ding, X., Jiang, Z., 2020. Scratch with double-tip tool: crack behavior during simultaneous double scratch on BK7 glass. *J. Eur. Ceram. Soc.* 40 (12), 4202–4216. <https://doi.org/10.1016/j.jeurceramsoc.2020.04.008>.
- Geng, Y., Yan, Y., Yu, B., Li, J., Zhang, Q., Hu, Z., Zhao, X., 2014. Depth prediction model of nano-grooves fabricated by AFM-based multi-passes scratching method. *Appl. Surf. Sci.* 313, 615–623. <https://doi.org/10.1016/j.apsusc.2014.06.033>.
- Gu, W., Yao, Z., Liang, X., 2011. Material removal of optical glass BK7 during single and double scratch tests. *Wear* 270 (3–4), 241–246. <https://doi.org/10.1016/j.wear.2010.10.064>.
- Huang, H., Li, X., Mu, D., Lawn, B., 2021. Science and art of ductile grinding of brittle solids. *Int. J. Mach. Tools Manuf.* 161, 103675. <https://doi.org/10.1016/j.ijmactools.2020.103675>.
- Ikeshima, D., Miyamoto, K., Yonezu, A., 2019. Molecular deformation mechanism of polycarbonate during nano-indentation: Molecular dynamics simulation and experimentation. *Polymer* 173, 80–87. <https://doi.org/10.1016/j.polymer.2019.04.029>.
- Karkalos, N., Markopoulos, A., Kundrak, J., 2017. In: Outeiro, J., Poulachon, G. (Eds.), *Molecular Dynamics Model of Nano-metric Peripheral Grinding*, 58. 16th CIRP Conference on Modelling of Machining Operations, Cluny, France, pp. 281–286. <https://doi.org/10.1016/j.procir.2017.03.189>.
- Kumar, J., 2013. Ultrasonic machining-a comprehensive review. *Mach. Sci. Technol.* 17 (3), 325–379. <https://doi.org/10.1080/10910344.2013.806093>.
- Li, J., Fang, Q., Zhang, L., Liu, Y., 2015. Subsurface damage mechanism of high speed grinding process in single crystal silicon revealed by atomistic simulations. *Appl. Surf. Sci.* 324, 464–474. <https://doi.org/10.1016/j.apsusc.2014.10.149>.
- Lin, J., Feng, J., Wen, Q., Wu, Y., Lu, J., Tian, Z., Wang, N., 2021. Deformation anisotropy of nano-scratching on C-plane of sapphire: a molecular dynamics study and experiment. *Appl. Surf. Sci.* 546, 149091. <https://doi.org/10.1016/j.apsusc.2021.149091>.
- Lu, J., Luo, Q., Xu, X., Huang, H., Jiang, F., 2019. Removal mechanism of 4H- and 6H-SiC substrates (0001 and 0001) in mechanical planarization machining. *Proc. Inst. Mech. Eng. Part B - J. Eng. Manuf.* 233 (1), 69–76. <https://doi.org/10.1177/0954405417718595>.
- Meng, B., Zhang, Y., Zhang, F., 2016. Material removal mechanism of 6H-SiC studied by nano-scratching with Berkovich indenter. *Appl. Phys. A Mater. Sci. Process.* 122 (3), 247. <https://doi.org/10.1007/s00339-016-9802-7>.
- Meng, B., Yuan, D., Xu, S., 2019. Coupling effect on the removal mechanism and surface/subsurface characteristics of SiC during grinding process at the nanoscale. *Ceram. Int.* 45 (2), 2483–2491. <https://doi.org/10.1016/j.ceramint.2018.10.175>.
- Peng, Q., Meng, F., Yang, Y., Lu, C., Deng, H., Wang, L., De, S., Gao, F., 2018. Shockwave generates < 100 > dislocation loops in bcc iron. *Nat. Commun.* 9, 4880. <https://doi.org/10.1038/s41467-018-07102-3>.
- Plimpton, S., 1995. Fast parallel algorithms for short-range molecular dynamics. *J. Comput. Phys.* 117, 1–19. <https://doi.org/10.1006/jcph.1995.1039>.
- Qiu, Z., Liu, C., Wang, H., Yang, X., Fang, F., Tang, J., 2016. Crack propagation and the material removal mechanism of glass-ceramics by the scratch test. *J. Mech. Behav. Biomed. Mater.* 64, 75–85. <https://doi.org/10.1016/j.jmbm.2016.07.021>.
- Qu, W., Wang, K., Miller, M., Huang, Y., Chandra, A., 2000. Using vibration-assisted grinding to reduce subsurface damage. *Precis. Eng.* 24 (4), 329–337. [https://doi.org/10.1016/S0141-6359\(00\)00043-X](https://doi.org/10.1016/S0141-6359(00)00043-X).
- Sharma, A., Kalsia, M., Uppal, A.S., Babbar, A., Dhawan, Vikas, 2021. Machining of hard and brittle materials: a comprehensive review. *Mater. Today Proc.* <https://doi.org/10.1016/j.matpr.2021.07.452>.
- Shimizu, J., Zhou, L., Eda, H., 2006. Molecular dynamics simulation of vibration-assisted cutting: influences of vibration parameters. *Int. J. Manuf. Technol. Manag.* 9 (1), 120–129. <https://doi.org/10.1504/IJMTM.2006.009990>.
- Stukowski, A., 2010. Visualization and analysis of atomistic simulation data with OVITO—the open visualization tool. *Model. Simul. Mater. Sci. Eng.* 18 (1), 015012. <https://doi.org/10.1088/0965-0393/18/1/015012>.
- Tersoff, J., 1989. Modeling solid-state chemistry: Interatomic potentials for multicomponent systems. *Phys. Rev.* 39 (8), 5566–5568. <https://doi.org/10.1103/PhysRevB.41.3248.2>.
- Tian, Z., Chen, X., Xu, X., 2020. Molecular dynamics simulation of the material removal in the scratching of 4H-SiC and 6H-SiC substrates. *Int. J. Extrem. Manuf.* 2 (4), 045104. <https://doi.org/10.1088/2631-7990/abc26c>.

- Wang, P., Ge, P., Ge, M., Bi, W., Meng, J., 2019. Material removal mechanism and crack propagation in single scratch and double scratch tests of single-crystal silicon carbide by abrasives on wire saw. *Ceram. Int.* 45 (1), 384–393. <https://doi.org/10.1016/j.ceramint.2018.09.178>.
- Wen, Y., Tang, J., Zhou, W., Zhu, C., 2019. Study on contact performance of ultrasonic-assisted grinding surface. *Ultrasonics* 91, 193–200. <https://doi.org/10.1016/j.ultras.2018.08.009>.
- Wu, Y., Mu, D., Huang, H., 2020. A Deformation and removal of semiconductor and laser single crystals at extremely small scales. *Int. J. Extrem. Manuf.* 2 (1), 012006 <https://doi.org/10.1088/2631-7990/ab7a2a>.
- Yang, X., Gao, S., 2022. Analysis of the crack propagation mechanism of multiple scratched glass-ceramics by an interference stress field prediction model and experiment. *Ceram. Int.* 48 (2), 2449–2458. <https://doi.org/10.1016/j.ceramint.2021.10.026>.
- Yang, X., Qiu, Z., Li, X., 2019a. Investigation of scratching sequence influence on material removal mechanism of glass-ceramics by the multiple scratch tests. *Ceram. Int.* 45 (1), 861–873. <https://doi.org/10.1016/j.ceramint.2018.09.256>.
- Yang, Z., Yang, Z., Zhu, L., Lin, B., Zhang, G., Ni, C., Sui, T., 2019b. The grinding force modeling and experimental study of ZrO₂ ceramic materials in ultrasonic vibration assisted grinding. *Ceram. Int.* 45 (7), 8873–8889. <https://doi.org/10.1016/j.ceramint.2019.01.216>.
- Zhang, P., Zhao, H., Shi, C., Zhang, L., Huang, H., Ren, L., 2013. Influence of double-tip scratch and single-tip scratch on nano-scratching process via molecular dynamics simulation. *Appl. Surf. Sci.* 280, 751–756. <https://doi.org/10.1016/j.apsusc.2013.05.056>.
- Zheng, F., Kang, R., Dong, Z., Guo, J., Liu, J., Zhang, J., 2018. A theoretical and experimental investigation on ultrasonic assisted grinding from the single-grain aspect. *Int. J. Mech. Sci.* 148, 667–675. <https://doi.org/10.1016/j.ijmecsci.2018.09.026>.
- Zhou, P., Shi, X., Li, J., Sun, T., Zhu, Y., Wang, Z., Chen, J., 2019. Molecular dynamics simulation of SiC removal mechanism in a fixed abrasive polishing process. *Ceram. Int.* 45 (12), 14614–14624. <https://doi.org/10.1016/j.ceramint.2019.04.180>.
- Zhou, W., Tang, J., Chen, H., Shao, W., 2019b. A comprehensive investigation of surface generation and material removal characteristics in ultrasonic vibration assisted grinding. *Int. J. Mech. Sci.* 156, 14–30. <https://doi.org/10.1016/j.ijmecsci.2019.03.026>.